Journal of ELECTRONIC MATERIALS, Vol. 44, No. 1, 2015
DOI: 10.1007/s11664-014-3406-9

Effects of Mg Doping on the Performance of InGaN Films Made by Reactive Sputtering

DONG-HAU KUO,[1,2] CHENG-CHE LI,[1] THI TRAN ANH TUAN,[1] and WEI-CHUN YEN[1]

1.—Department of Materials Science and Engineering, National Taiwan University of Science and Technology, Taipei 10607, Taiwan. 2.—e-mail: dhkuo@mail.ntust.edu.tw

Mg-doped InGaN (Mg-InGaN) films have been deposited directly on Si (100) substrates by radio-frequency reactive sputtering technique with single cermet targets in an Ar/N_2 atmosphere. The cermet targets with a constant 5% indium content were made by hot pressing the mixture of metallic In, Ga, and Mg powders and ceramic GaN powder. The Mg-InGaN films had a wurtzite structure with a preferential $(10\bar{1}0)$ growth plane. The SEM images showed that Mg-InGaN films were smooth, continuous, free from cracks and holes, and composed of nanometer-sized grains. As the Mg dopant content in Mg-InGaN increased to 7.7 at.%, the film was directly transformed into *p*-type conduction without a post-annealing process. It had high hole concentration of 5.53×10^{18} cm^{-3} and electrical mobility of 15.7 ± 4.2 cm^2 V^{-1} s^{-1}. The overdoping of Mg in InGaN degraded the electrical properties. The bandgap of Mg-InGaN films decreased from 2.92 eV to 2.84 eV, as the Mg content increased from 7.7% to 18.2%. The constructed *p*-type Mg-InGaN/*n*-type GaN diode was used to confirm the realization of the *p*-type InGaN by sputtering technique.

Key words: *p*-type InGaN, thin film, sputtering, electrical property

INTRODUCTION

In the past few decades, III-nitride semiconductors such as AlN, GaN, InN, and their alloys have been widely investigated for electro-optical device applications. The III-nitride semiconductors showed a direct bandgap of 0.65 eV for InN, 3.4 eV for GaN, and 6.2 eV for AlN.[1–3] In addition, the most potential III-nitride is InGaN alloy, whose light emission can be controlled from near-ultraviolet to infrared by adjusting the composition ratio of In and Ga.[4] The InGaN film had many advantages such as high breakdown voltage and high electron mobility, which has made it widely used in light-emitting diodes (LEDs) and high electron mobility transistors (HEMTs).[5–7]

Mg-doped *p*-GaN film is also an important material for development LEDs or power effect devices. In general, high hole concentrations in the *p*-GaN layer promote the light emission of LEDs. The research in *p*-GaN began in the early 1990s by Nakamura et al. [8] Their *p*-GaN film was deposited by metal organic chemical vapor deposition (MOCVD) followed by annealing at 700°C in N_2 atmosphere. The *p*-GaN film was activated by an annealing processing which decreased the resistivity from 1×10^6 Ω cm to 2 Ω cm with a hole concentration of 3×10^{17} cm^{-3}. Furthermore, there are several approaches to increase the hole concentration of *p*-GaN films, such as *δ*-doping,[9] multilayered buffer,[10] and Mg–O co-doping.[11]

However, Mg-doped InGaN exhibits a higher hole concentration than Mg-doped GaN due to the lower activation energy of Mg acceptors within a decreased bandgap energy.[12,13] The Mg ionization energy is about 125–215 meV, which indicates that only several percent of Mg acceptors can be activated to form hole carriers. It also means that heavy Mg doping is required. Regrettably, the heavy doping may decrease hole concentration due to the self-compensation effect.[14] Additionally, *p*-InGaN showed other characteristics such as low contact resistance, low etching damage and lower deposition

(Received July 12, 2014; accepted September 1, 2014; published online September 18, 2014)

temperature than *p*-GaN.[15] So far, most *p*-InGaN films have been grown at 680–1050°C by MOCVD, which showed a high hole concentration of 10^{18}–10^{19} cm^3.[13,16] However, there are no reports on the growth of *p*-InGaN films by sputtering technique.

In this work, we successfully deposited *p*-InGaN films by radio-frequency (rf) sputtering with single cermet targets. The cermet targets were made by hot pressing the mixture of metallic Mg, In, and Ga and ceramic GaN powders. The GaN content was more than 50% to provide solid support in the targets. A high hole concentration of *p*-InGaN films can be deposited by this method without an annealing process. The formation of the Mg–H bonding can be avoided by the sputtering technique due to the hydrogen-free process condition. On the other hand, this method provides a cheap and environmentally safe approach for the electronic applications in the future.

EXPERIMENTAL PROCEDURES

Mg-InGaN films were deposited on Si (100) substrates by rf reactive sputtering technique with single cermet targets in a ($Ar + N_2$) atmosphere. The 2-inch (c.5-cm) cermet targets were prepared by hot pressing the mixture of metallic In, Ga, and Mg powders and ceramic GaN powder. The In content in each Mg-doped target was kept at 5 at.%, while there were different Mg contents at 0 at.%, 10 at.%, 15 at.%, and 20 at.%. Their corresponding films were symbolized as Mg-*x*-InGaN with $x = 0$, 0.1, 0.15, and 0.2. Before sputtering, the chamber pressure was pumped to 1×10^{-6} torr by diffusion pump to avoid the oxygen and impurities. The deposition temperature was kept at 400°C. The rf sputtering power and working pressure was kept at 150 W and 9×10^{-3} torr, respectively. The deposition time was 60 min. The sputtering process was under the gas mixture of Ar and N_2 with a flow rate of 5 sccm for each.

The crystal structure of Mg-InGaN films was analyzed by x-ray diffractometry (XRD; D8 Discover, Bruker) and high–resolution transmission electron microscopy (HRTEM; Technai G2, Philips). The surface morphological images of Mg-InGaN films were observed by scanning electron microscopy (SEM; JSM-6500F, JEOL) and atomic force microscopy (AFM; Dimension Icon, Bruker). An energy dispersive spectrometer (EDS; JSM-6500F, JEOL) equipped on SEM was used for composition analysis. The electrical properties were measured by Hall effect measurement (HMS-2000, Ecopia) at room temperature with a maximum magnetic field of 0.51 T. Before the Hall effect measurement, the samples had four electrical contacts made of silver paste, which was dried in an oven at 100°C for 10 min. A ultraviolet–visible (UV–vis) spectrometer (V-670, Jasco) was used to measure the absorption spectra for Mg-InGaN films deposited on the transparent glass substrates.

RESULTS AND DISCUSSION

Table I shows the EDS composition analyses of Mg-*x*-InGaN films at different Mg contents. The [N]/([In] + [Ga] + [Mg]) ratios were 0.87, 0.95, 0.81 and 0.84 for Mg-*x*-InGaN films at $x = 0$, 0.1, 0.15, and 0.20, respectively. For Mg-*x*-InGaN at $x = 0.1$, its composition was close to a stoichiometric ratio of 1. However, all nitrogen contents in the Mg-InGaN films were less than 50 at.%, which indicated that Mg-InGaN films were in a nitrogen-deficient state. The [Mg]/([In] + [Ga] + [Mg]) ratios were 0.077, 0.127, and 0.182, as the Mg contents in cermet targets were 10 at.%, 15 at.%, and 20 at.%, respectively. The Mg contents in Mg-InGaN films were slight less than those in the targets. With the increase in the Mg content, the film decreased its Ga content in return. For the In content, the expected In ratios were expected to be 0.05. However, the [In]/([In] + [Ga] + [Mg]) ratios were 0.116, 0.057, 0.069, and 0.069 for Mg-*x*-InGaN at 0, 0.1, 0.15, and 0.2., respectively. The Mg-free InGaN film had the relatively high In content of 0.116 with a large deviation from 0.05. With the incorporation of Mg, the In content becomes relatively consistent with the design composition. This composition data indicate that the Mg incorporation into InGaN target can have the film growth with a better composition control. The large deviation in the In content for the Mg-free InGaN film can be attributed to the melt flow of In during target preparation.

Figure 1 shows XRD patterns of the Mg-*x*-InGaN films at $x = 0$, 0.1, 0.15, and 0.2. In this work, the Mg-*x*-InGaN films deposited on Si (100) substrates all exhibited a wurtzite structure. For undoped InGaN, the crystallinity was close to single crystal and the preferentially $(10\bar{1}0)$-oriented peak was clearly observed at $2\theta = 32.05^{\circ}$ due to the $(10\bar{1}0)$ plane with a lower surface energy than other crystal

Table I. Compositional analyses of Mg-*x*-InGaN films at $x = 0$, 0.1, 0.15, and 0.2

Mg-*x*-InGaN films	In (at.%)	Ga (at.%)	Mg (at.%)	N (at.%)	[Mg]/([In] + [Ga] + [Mg])	[In]/([In] + [Ga] + [Mg]	[N]/([In] + [Ga] + [Mg])
$x = 0$	6.20	47.2	–	46.7	–	0.116	0.874
$x = 0.1$	2.93	44.3	3.95	48.8	0.077	0.057	0.953
$x = 0.15$	3.79	44.3	7.01	44.9	0.127	0.069	0.814
$x = 0.20$	3.78	40.7	9.91	45.6	0.182	0.069	0.838

planes.[17] As the pure GaN has the $(10\bar{1}0)$ peak located at $2\theta = 32.38^{\circ}$,[18] there is a peak shift to the lower diffraction angle due to the substitution of small gallium ion by the larger indium ion. The In content of undoped $In_yGa_{1-y}N$ film can be calculated from the $(10\bar{1}0)$ peak shift by Vegard's Law as shown below

$$2\theta_{InGaN} = y \times 2\theta_{InN} + (1-y) \times 2\theta_{GaN}, \qquad (1)$$

where θ_{InGaN}, θ_{InN}, and θ_{GaN} are the diffraction angles of $(10\bar{1}0)$ lattice plane for InGaN, InN, and GaN, respectively. The y value of InGaN film was calculated to be 0.10, which is close to the EDS result of 11.6% for the undoped InGaN film. Furthermore, the Mg-InGaN films became polycrystalline and the $(10\bar{1}0)$ peak were shifted to around $2\theta = 31.85°$ as the Mg dopant was added into InGaN films. Basically, the main substitution of the smaller Ga^{3+} ion [$r(Ga^{3+}) = 0.62$ Å of effective ionic radius] in GaN with the larger Mg^{2+} ion [$r(Mg^{2+}) = 0.72$ Å] leads to the lattice expansion and the shift of diffraction peak to a smaller 2θ value.[19] Besides, the $(10\bar{1}1)$ peak intensity increased as the Mg dopant content increased, and the diffraction peaks from the $(11\bar{2}0)$ and $(20\bar{2}0)$ planes also showed up, which could be attributed to the lattice distortion. XRD patterns showed that none of the Mg-InGaN films had phase separation or secondary phases. It is apparent that the Mg dopant completely dissolves into InGaN to form a solid solution, which indicates that the Mg cation substitutes the lattice site of the Ga cation. The result of solid solutioning proves that the Mg-InGaN films have been successfully developed by rf reactive sputtering with a single cermet target.

The structure property of the Mg-0.15-InGaN film was also investigated by high-resolution TEM (HRTEM). As shown in Fig. 2, the Mg-0.15-InGaN film behaved as polycrystalline. Its d-space value was calculated to be 2.81 Å, which corresponded to the $(10\bar{1}0)$ crystalline plane. Inset the selected area electron diffraction (SAED) pattern of Mg-0.1-InGaN film. This film exhibited a polycrystalline structure and the $(10\bar{1}0)$, $(10\bar{1}1)$, and $(11\bar{2}0)$ crystal planes could be observed from the SAED pattern, which is consistent with the XRD results.

Figure 3 shows SEM surface and cross-sectional images of Mg-x-InGaN films deposited at 400°C by rf sputtering. These images showed that Mg-InGaN films were smooth, continuous, free from cracks and holes, and composed of nanometer-sized grains. The grain sizes were 33.5 ± 2.0 nm, 48.6 ± 1.3 nm, 58.4 ± 1.1 nm, and 68.2 ± 5.1 nm for Mg-x-InGaN films at $x = 0$, 0.1, 0.15, and 0.2, respectively. The addition of Mg dopant into InGaN films obviously enhanced the grain growth. The cross-sectional images are individually shown in the insets. The columnar structure in InGaN and Mg-InGaN films were not obvious due to the low thermal stability of In at 400°C and lattice distortion from the Mg incorporation. In addition, the thermal expansion coefficient of InGaN, combining from GaN (5.6×10^{-6} K^{-1}) and InN (3.8×10^{-6} K^{-1}),[20,21] was close to 5.5×10^{-6} K^{-1} after calculation by Vegard's law. The thermal expansion coefficients of Si substrate was 3.6×10^{-6} K^{-1}.[20] Although there is a large difference in the thermal expansion coefficients between InGaN films and Si substrate, the cross-sectional images of Mg-InGaN films with thicknesses of 1.5–2 μm do not show the interfacial cracking and film cracking, which can be attributed to the polycrystalline nature of the preferentially oriented Mg-InGaN films.

Figure 4 shows the AFM morphologies of Mg-InGaN films after scanning on the 5×5 μm^2 dimension. The root-mean-square (rms) roughness

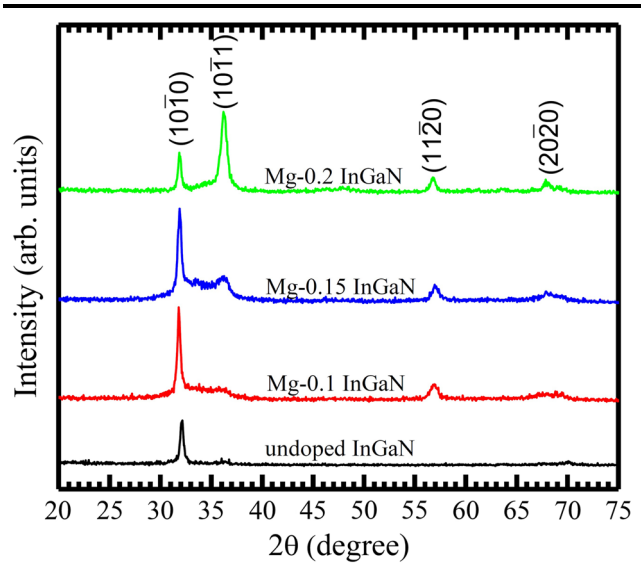

Fig. 1. XRD pattern of Mg-x InGaN films deposited at 400°C in Ar/N2 atmosphere with different Mg-dopant contents in cermet targets.

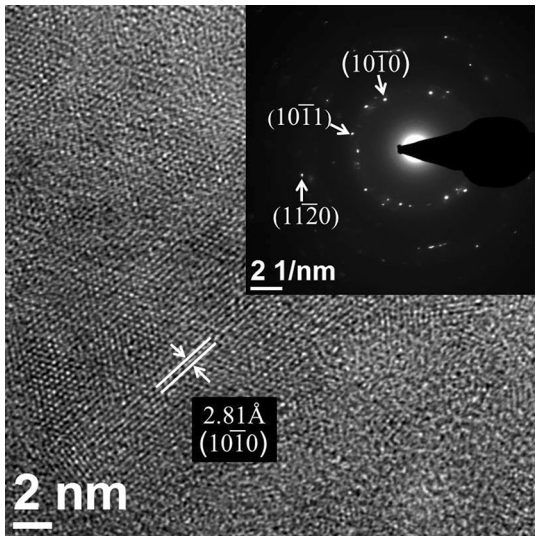

Fig. 2. HRTEM micrograph of Mg-0.15 InGaN film deposited at 400°C in Ar/N2 atmosphere. Inset the SEAD pattern of Mg-0.15 InGaN film.

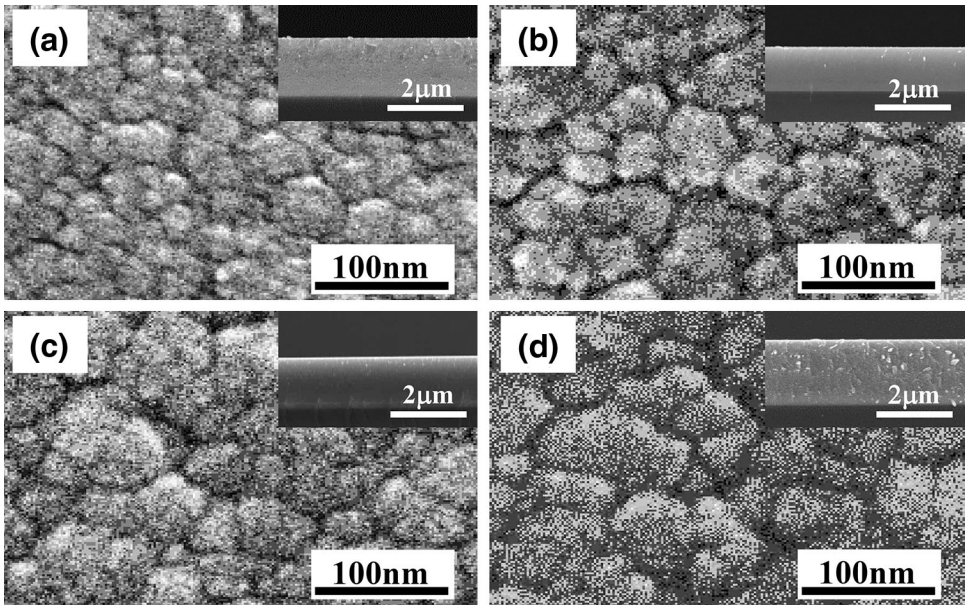

Fig. 3. SEM surface images of Mg-x-InGaN films at x = (a) 0, (b) 0.1, (c) 0.15, and (d) 0.2. Insets their individual cross-sectional images.

of undoped InGaN film was 2.33 nm. After incorporating the Mg dopants into the InGaN films, the rms roughness of Mg-x-InGaN films increased to 3.12 nm, 3.67 nm, and 4.75 nm for x = 0.1, 0.15, and 0.2, respectively. The roughness increased with the increase in the Mg content. Our rms values were also larger than the films grown by MOCVD with roughness of 0.6–1.1 nm.[22,23] The rougher surface for our Mg-InGaN films was caused by the lower deposition temperature at 400°C, which cannot provide sufficient kinetic energy for the adatoms to grow into an epitaxial layer, instead forming the polycrystalline films.

Electrical properties of Mg-x-InGaN films at x = 0, 0.1, 0.15, and 0.2 were measured by Hall effect measurement at room temperature. The carrier concentration, mobility, and electrical conductivity are shown in Fig. 5. The undoped InGaN films deposited at 400°C showed as a n-type semiconductor. The carrier concentration and mobility were 1.06×10^{19} cm^{-3} and 12.6 ± 3.3 cm^2 V^{-1} s^{-1}, respectively. As the Mg dopant content increased to 7.7 at.% in the Mg-0.1-InGaN film, this film directly transformed into p-type conduction without a thermal annealing process. The Mg-0.1-InGaN film showed high hole concentration of 5.53×10^{18} cm^{-3} and the mobility slightly increased to 15.7 ± 4.2 cm^2 V^{-1} s^{-1}. As the Mg content increased to 12.7 at.% for Mg-0.15-InGaN film, the film still remained as a p–type semiconductor with hole concentration of 1.29×10^{17} cm^{-3} and mobility of 4.0 ± 1.5 cm^2 V^{-1} s^{-1}. As the Mg content increased to 18.2 at.% for Mg-0.2-InGaN film, the hole concentration and mobility decreased to 9.83×10^{16} cm^{-3} and 3.7 ± 1.4 cm^2 V^{-1} s^{-1}, respectively. The n-to-p transition supports the solid solutioning of Mg^{2+} dopant into the B^{3+} site. If Mg^{2+}does not substitute the B^{3+} site, it will behave as an impurity and precipitate as Mg nitride to block the charge transport across the grain boundary. In our previous report of Mg-0.1-GaN film instead of InGaN, the hole concentration and mobility was 9.37×10^{16} cm^{-3} and 345 cm^2 V^{-1} s^{-1}, respectively.[24] However, in this study, the Mg-0.1-InGaN film showed high hole concentration of 5.53×10^{18} cm^{-3} and the much lower mobility of 15.7 ± 4.2 cm^2 V^{-1} s^{-1}. The drop in mobility is caused by the high hole concentration.

The change in carrier concentration with the Mg incorporation into InGaN is strongly related to the film composition, as shown in Table I. Although the nitrogen deficiency generates the nitrogen vacancies (V_N) as the donor defect to enhance the electron concentration, the high electron concentration for Mg-free InGaN is mainly attributed to the high In content. Kumakura et al. found that hole concentration of Mg-$In_{0.04}Ga_{0.96}N$ film made by MOVPE was 5.3×10^{18} cm^{-3}.[25] Our hole concentration was close to theirs, despite their Mg dopant having better solubility with higher temperature process at 780°C instead of ours at 400°C. In this work, the sputtering plasma can provide Mg dopant with sufficient energy for it to dissolve into the InGaN lattice and have the same ability, similar to the MOCVD technique for Mg-doped InGaN film, in Mg solubility, even though our deposition temperature was only 400°C.

The conductivity of Mg-InGaN films depends on carrier concentration and mobility. As we can see, the undoped InGaN film had a highest conductivity of 20.3 S cm^{-1} due to the high electron concentration of $\sim 10^{19}$ cm^{-3}. As the Mg dopant content increased to 7.7 at.%, 12.7 at.%, and 18.2 at.%, the conductivity dropped to 7.13 S cm^{-1}, 0.08 S cm^{-1},

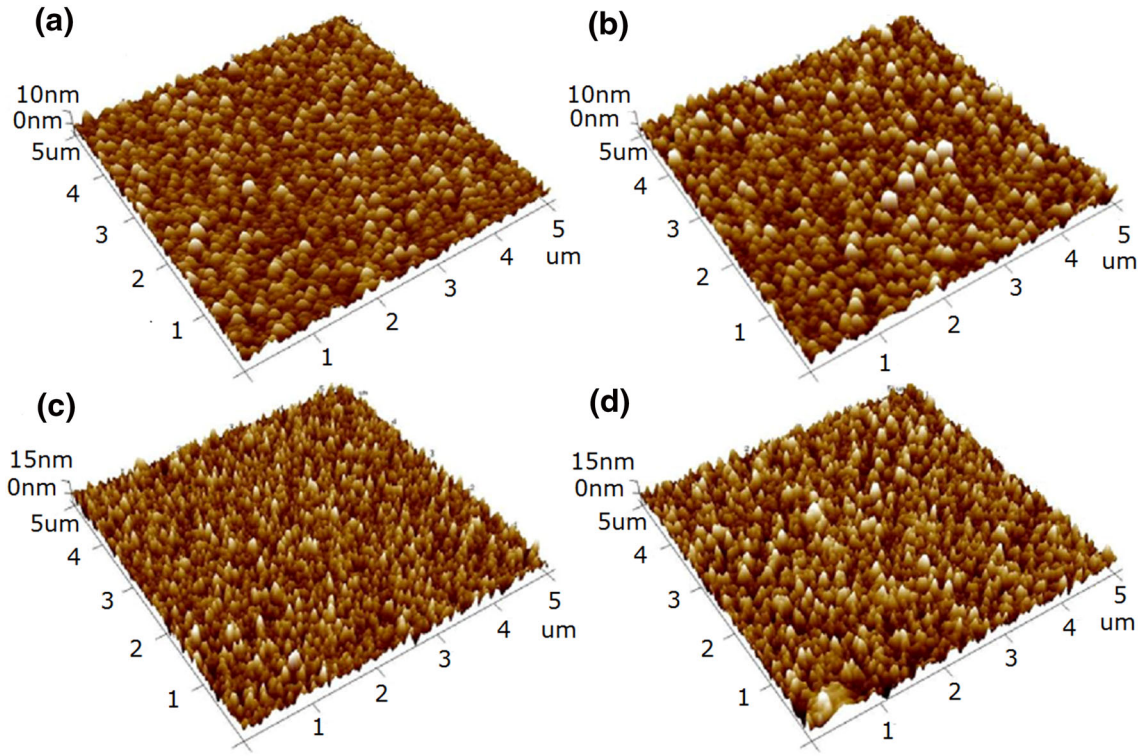

Fig. 4. AFM morphologies with 5 × 5 m^2 scans of Mg-*x*-InGaN films at *x* = (a) 0, (b) 0.1, (c) 0.15, and (d) 0.2.

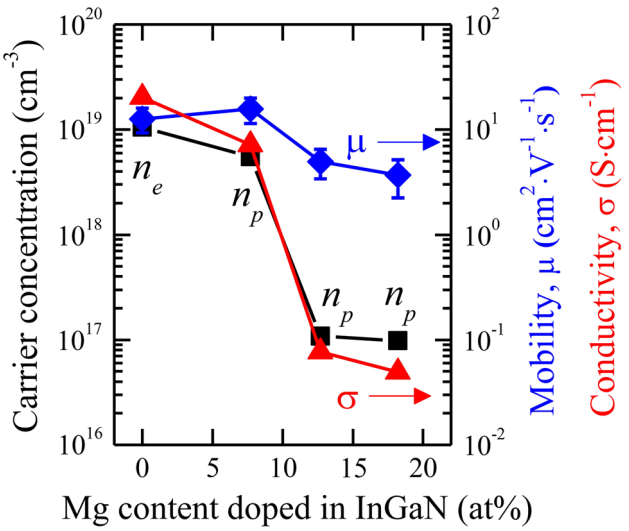

Fig. 5. Electrical properties of carrier concentration, mobility, and electrical conductivity for Mg-InGaN films deposited at 400°C with different Mg contents.

and 0.05 S cm^{-1}, respectively. The excess Mg dopant precipitated at the grain boundary and formed Mg_3N_2, which retarded the electrical transport and increased the resistivity. For MOCVD Mg-InGaN, thermal annealing is needed to activate the Mg dopant and break the Mg–H bonding for improved electrical conductivity.[26] Nevertheless, in this work, the *p*–type Mg-InGaN film can be deposited by rf sputtering without an annealing process and still maintain the good conductivity. The sputtering technique did not use the metalorganic species and hydrogen atmosphere which can prevent the formation of the Mg–H bonding.

For the effect of Mg dopant on electrical concentration, it is expected that the higher Mg content of Mg-*x*-InGaN can provide more acceptors and more hole concentration. In contrast, the hole concentration drops from 5.53×10^{18} cm^{-3} at $x = 0.1$ to 1.29×10^{17} cm^{-3} at $x = 0.15$ and 9.83×10^{16} cm^{-3} at $x = 0.2$. This information indicates that the Mg content in films does not all enter into the IIIB site to form a solid solution. Mg in InGaN has its maximal solubility changed with the indium content. If its doping content is more than it can dissolve, the excessive Mg content will be nitridized and become precipitates at the grain boundaries. This precipitate surrounds the grain boundaries and can retard the carrier transport and lower the electrical conductivity and carrier concentration. The other possible reason is the increased point defect associates from the increased extrinsic dopants to act as charge traps to lower carrier concentration.

UV–vis measurements of Mg-InGaN films were executed at room temperature. From the UV–vis spectrum results, the bandgap (E_g) of Mg-InGaN films could be calculated by the Tauc equation which expressed as Eq. 2[27]

$$(\alpha h\upsilon)^2 = A(h\upsilon - E_g) \qquad (2)$$

where α is optical absorption coefficient, A a constant, $h\upsilon$ the incident photon energy, and E_g the energy bandgap of the Mg-InGaN films. The bandgap of Mg-InGaN films can be obtained directly by plotting the $(\alpha h\upsilon)^2 - h\upsilon$ curves, followed by extrapolating the linear part of the curves, as shown in Fig. 6. The obtained E_g values were 2.97 eV, 2.92 eV, 2.88 eV, and 2.84 eV for Mg-x-InGaN at x = 0, 0.1, 0.15, and 0.2, respectively. The Mg-InGaN films were in a nitrogen deficiency state, as proved by the previous EDS results. The nitrogen vacancy (V_N) has been reported as the dominant defect in GaN with shallow donor level, which decreases the bandgap of the films.[28,29] However, Kumakura et al. found that Mg doping does not significantly affect the E_g value due to its acceptor level being only 0.1–0.17 eV above the valence band maximum.[15] The bandgap of Mg-doped $In_{0.06}Ga_{0.94}N$ films grown by MOVPE was only 2.45 eV. In this study, the change in bandgap was 80 meV for Mg-InGaN films with the Mg content increasing from 7.7 at.% to 18.2 at.%.

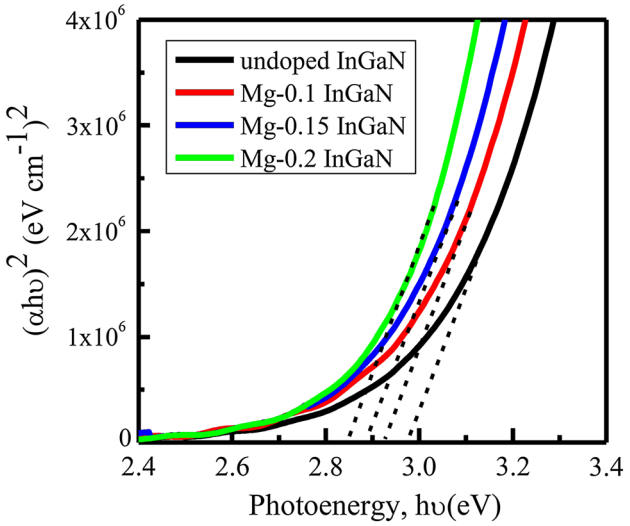

Fig. 6. Plots of $(\alpha h\upsilon)2$ versus photon energy ($h\upsilon$) for the optical bandgap determination of the Mg-x-InGaN films (x = 0, 0.1, 0.15 and 0.2) deposited at 400°C on transparent glass substrates.

From our experiments, we have proved the possibility of using reactive sputtering to prepare p-type InGaN films. p-type GaN is the major p-type for III-V nitride semiconductors for electro-optic applications such as LED. Undoped n-type InGaN has been grown as the n-type for LED. Little p-type InGaN has been applied for electronic applications, because the lower growth temperature for MOCVD-made InGaN instead of GaN is not favored for incorporating Mg into the IIIB site of InGaN. Our low temperature process at 400°C has avoided the indium vaporization and our plasma also provides sufficient kinetic energy to incorporate Mg into InGaN. By reactive sputtering, the process for p-type InGaN becomes cheap, safe at low growth temperature and without combustible precursors and toxic ammonia, and simple with no need for post-annealing. p-type InGaN-based electronic devices instead of n-type InGaN ones will provide much more diversity in III-V nitride devices.

To support our Mg-InGaN being p-type, a p/n junction with the structural modeling shown in Fig. 7a is presented. The p/n junction diode was made by rf reactive sputtering with the selections of GaN for n-layer and Mg-0.1-InGaN (with doping Mg of 10%) for the p-layer. The p-Mg-InGaN film was deposited on the $Pt/TiO_2/Si$ substrate at 400°C under rf power of 150 W for 40 min. After depositing p-type Mg-InGaN film, the n-type GaN film was grown at 200°C under rf power of 120 W for 40 min. The Al layer on the top was sputtered at 200°C for 30 min with a pure Al target. Pt and Al were the electrodes of the p/n junction diode. The cross-sectional SEM image of the p/n junction diode shown in the Fig. 7b has a smooth p-Mg-InGaN layer and a columnar n-GaN layer. With SEM analysis, the thicknesses of the Pt and Al layers were found to be ~220 nm and 280 nm, respectively. The thicknesses of the n-type GaN and p-type Mg-InGaN and films were calculated to be 0.65 μm and 1.0 μm, respectively. Figure 8 shows the current–voltage (I–V) characteristics of the

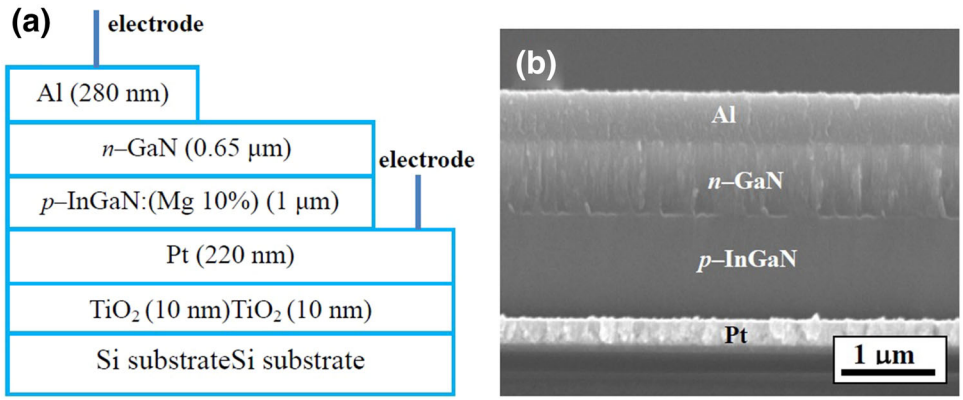

Fig. 7. (a) The structural modeling and (b) the cross-sectional SEM image of the p/n junction diode.

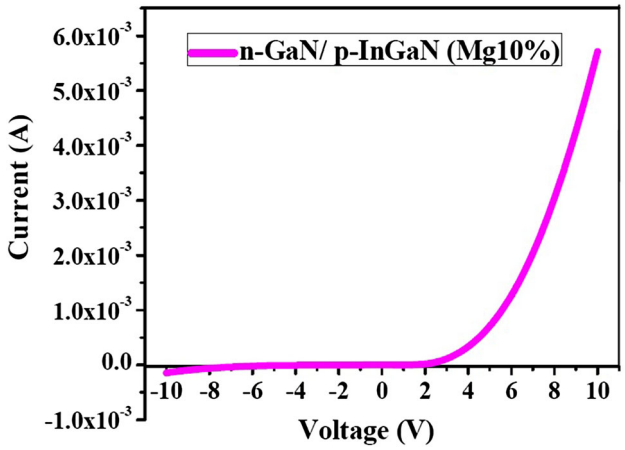

Fig. 8. Electrical properties of the *p*/*n* junction diode measured at room temperature.

diode tested at room temperature. The leakage current of the p/n junction diode was found to be 3.08×10^{-7} A under the reverse bias of -1 V. This diode also showed the turn-on voltage of $\sim$1.9 V and the breakdown voltage of > -10 V. With the rectifying behavior, the diode is confirmed to be built with a *p*/*n* junction.

CONCLUSIONS

Mg-InGaN films have been successful deposited on Si (100) substrates by rf reactive sputtering technique with single cermet targets. XRD, TEM, SEM, AFM, and UV–vis spectrometry were used to investigate the microstructure and characterizations of Mg-InGaN films. Mg-InGaN films had polycrystalline and wurtzite structure. They became *p*-type at the 7.7% Mg doping content without the need of a post-annealing process, with A high hole concentration of 5.53×10^{18} cm^{-3} and the mobility of 15.7 ± 4.2 cm^2 V^{-1} s^{-1}. At the higher Mg content, the electrical properties of Mg-InGaN degraded due to the solubility limitation. The success in *p*-type InGaN has facilitated the fabrication of *p*/*n* diode devices with a low-cost and environmentally friendly process.

ACKNOWLEDGEMENT

This work was supported by the Ministry of Science and Technology of the Republic of China under Grant numbers 102-2221-E-011-019-MY2 and 103-ET-E-011-008-ET.

REFERENCES

1. O. Ambacher, *J. Phys. D* 31, 2653 (1998).
2. C.S. Gallinat, G. Koblmüller, J.S. Brown, S. Bernardis, J.S. Speck, G.D. Chern, E.D. Readinger, H. Shen, and M. Wraback, *Appl. Phys. Lett.* 89, 032109 (2006).
3. J. Wan, R. Venugopal, M.R. Melloch, H.M. Liaw, and W.J. Rummel, *Appl. Phys. Lett.* 79, 1459 (2001).
4. B. Liu, W. Luo, R. Zhang, Z. Zou, Z. Xie, Z. Li, D. Chen, X. Xiu, P. Han, and Y. Zheng, *Phys. Status Solidi C* 7, 1817 (2010).
5. S.C. Jain, M. Willander, J. Narayan, and R. Van Overstraeten, *J. Appl. Phys.* 87, 965 (2000).
6. W. Lanford, V. Kumar, R. Schwindt, A. Kuliev, I. Adesida, A.M. Dabiran, A.M. Wowchak, P.P. Chow, and J.W. Lee, *Eelectron. Lett.* 40, 771 (2004).
7. N. Okamoto, K. Hoshino, N. Hara, M. Takikawa, and Y. Arakawa, *J. Cryst. Growth* 272, 278 (2004).
8. S. Nakamura, T. Mukai, M. Senoh, and N. Iwasa, *Jpn. J. Appl. Phys.* 31, 139 (1992).
9. Y. Chen, H. Wu, G. Yue, Z. Chen, Z. Zheng, Z. Wu, G. Wang, and H. Jiang, *Appl. Phys. Express* 6, 041001 (2013).
10. X. Zhang, S.J. Chua, P. Li, K.B. Chong, and W. Wang, *Appl. Phys. Lett.* 73, 1772 (1998).
11. G. Kipshidze, V. Kuryatkov, B. Borisov, Y. Kudryavtsev, R. Asomoza, S. Nikishin, and H. Temkin, *Appl. Phys. Lett.* 80, 2910 (2002).
12. L. Sang, M. Takeguchi, W. Lee, Y. Nakayama, M. Lozac'h, T. Sekiguchi, and M. Sumiya, *Appl. Phys. Express* 3, 111004 (2010).
13. B.N. Pantha, A. Sedhain, J. Li, J.Y. Lin, and H.X. Jiang, *Appl. Phys. Lett.* 95, 261904 (2009).
14. P. Kozodoy, H. Xing, S.P. DenBaars, U.K. Mishra, A. Saxler, R. Perrin, S. Elhamri, and W.C. Mitchel, *J. Appl. Phys.* 87, 1832 (2000).
15. K. Kumakura, T. Makimoto, and N. Kobayashi, *J. Appl. Phys.* 93, 3370 (2003).
16. P.C. Chen, C.H. Chen, S.J. Chang, Y.K. Su, P.C. Chang, and B.R. Huang, *Thin Solid Films* 498, 113 (2006).
17. J.E. Northrup, L.T. Romano, and J. Neugebauer, *Appl. Phys. Lett.* 74, 2319 (1999).
18. C.M. Balkasa, C. Basceria, and R.F. Davis, *Powder Diffr.* 10, 266 (1995).
19. R.D. Shannon and C.T. Prewitt, *Acta Cryst. B* 25, 925 (1969).
20. S. Strite and H. Morkoç, *J. Vac. Sci. Technol. B* 10, 1237 (1992).
21. K. Wang and R.R. Reeber, *Appl. Phys. Lett.* 79, 1602 (2011).
22. W. Lee, J. Limb, J.H. Ryou, D. Yoo, M.A. Ewing, Y. Korenblit, and R.D. Dupuis, *J. Display Technol.* 3, 126 (2007).
23. W. Lee, J. Limb, J.H. Ryou, D. Yoo, T. Chung, and R.D. Dupuis, *J. Cryst. Growth* 287, 557 (2006).
24. C.C. Li and D.H. Kuo, *J. Mater. Sci. Mater. Electron* 25, 1942 (2014).
25. K. Kumakura, T. Makimoto, and N. Kobayashi, *Jpn. J. Appl. Phys.* 39, 337 (2000).
26. K. Sasamoto, T. Hotta, K. Sugita, A.G. Bhuiyan, A. Hashimoto, A. Yamamoto, K. Kinoshita, and Y. Kohji, *J. Cryst. Growth* 318, 492 (2011).
27. S. Muthukumaran and R. Gopalakrishnan, *Opt. Mater.* 34, 1946 (2012).
28. I. Gorczyca, A. Svane, and N.E. Christensen, *Solid State Commun.* 101, 747 (1997).
29. M.G. Ganchenkova and R.M. Nieminen, *Phys. Rev. Lett.* 96, 196402 (2006).